Ultralow loading palladium nanocatalysts prepared by atomic layer deposition on three-dimensional graphite-coated nickel foam to enhanced ethanol electro-oxidation reaction

Yiwu Jiang, Jinwei Chen*, Jie Zhang, Anqi Li, Yaping Zeng, Feilong Zhou, Gang Wang, Ruilin Wang*

College of Materials Science and Engineering, Sichuan University, Chengdu 610065, China

* Corresponding author. Tel & Fax: +86 28 85418018.

E-mail address: jwchen@scu.edu.cn, rl.wang@scu.edu.cn

Abstract

A novel three-dimensional graphite-coated nickel foam (GNF) was synthesized by the chemical vapor deposition (CVD) method, and palladium nanoparticles (Pd NPs) were successfully synthesized on GNF support by metal atomic layer deposition (ALD) technology for the first time. The physicochemical properties of the as-prepared catalysts were characterized by X-ray diffraction (XRD), Raman Spectra, scanning electron microscope (SEM), energy dispersive X-ray spectrometer (EDS), X-ray photoelectron spectroscopy (XPS) and inductively coupled plasma-atomic emission epectrometry (ICP). Results showed that the Pd NPs with ultralow loading (below 50 $\mu g/cm^2_{Pd}$) were uniformly dispersed on GNF support, and the as-prepared catalysts presented the highest catalytic activity toward ethanol electro-oxidation (the peaking current density was about 39.97 mA/cm^2) in alkaline media. Especially, it was found that the morphology and content of graphite of GNF will greatly affect the

dispersing of ALD Pd NPs. When the CVD time for preparing GNF was 10 min, the as-prepared catalyst presented higher dispersity of Pd NPs and catalytic activity toward ethanol electro-oxidation than that of other as-prepared catalysts. The effect of ALD cycle for Pd NPs growth and its performance was also investigated. When cycle of ALD Pd was 450, the peaking current density of as-prepared catalysts was about 2.64 times as high as that of commercial Pd/C to ethanol electro-oxidation. Herein, there is a promising application prospect for the prepared Pd/GNF nanocomposite as an electrocatalyst toward ethanol electro-oxidation in alkaline media.

Introduction

In recent years, direct ethanol fuel cells (DEFCs) have triggered intensive attention, due to the several intrinsic advantages of ethanol, such as low cost, easy storage, low toxicity and pollutant emission, high energy density (8.01 KWh/Kg, 6.34 KWh/L), ease of handling and transport than hydrogen.[1-4] Besides, ethanol can be easily produced in large quantities by the fermentation of biomass from agriculture.[5, 6] So DEFCs has been deemed to promising power source. However, ethanol oxidation process involves cleavage of the C-C bond which is difficult to be implemented at low temperature.[7] The existing electrocatalysts have the low oxidation efficiency for ethanol and poor resistance to carbon monoxide (CO) poisoning. These issues will badly obstruct the practical applications of DEFCs.[8] Hence, the development of highly active electrocatalysts is very critical to achieving the commercialization of DEFCs.

Lots of research showed that ethanol presented higher oxidation reaction activity in alkaline medium than acid medium.[9, 10] Currently, palladium (Pd) is considered to be a promising alternative to platinum (Pt) on ethanol electro-oxidation in alkaline medium,[11] because Pd has several special advantages: cheaper, more abundant on the earth and higher tolerance to carbonaceous species from ethanol oxidation than Pt and high electroactive for ethanol oxidation.[6, 11, 12] However, it still needs to further promote the catalytic activity and durability of mono-Pd catalyst. It is well known that the support materials will greatly affect the performance of catalysts. Pd nanoparticles (NPs) or PdM (Ru, Sn, or Ir) were designed to disperse on various support such as carbon black,[13] reduced graphene oxide,[14] carbon nanotubes,[14-16] titanium dioxide,[17] three-dimensional graphite foam (3D-GF),[18-20] and so on.[21-23] Among these carbon supports, 3D-GF has been considered as promising carbon support because it has an excellent electrical conductivity, high mechanical flexibility, large surface area, and chemical stability and uniquely three-dimensional structure.[18, 24-26] In the Tsang's work,[19] Pd/graphene aerogel catalyst was deposited on nickel foam. The novel binder-free 3D electrode showed high performance for methanol electro-oxidation. Zhang et al.[18] researched a new Pd-graphene/NF catalyst in which graphene was deposited on nickel foam by chemical bath method as to the support of Pd NPs. The novel catalyst showed high activity for methanol oxidation. These excellent works demonstrated the advantage of 3D support. Herein, we try to in-situ grow graphene into 3D NF structure by chemical vapor deposition (CVD) as support for fuel cell catalyst.

Furthermore, how to effectively deposit noble metal nanoparticles into the 3D structure support? As we know that wet chemistry techniques is widely used for preparing fuel cell catalysts.[27] The noble metal nanocatalysts always are reduced by reducing agent under stirring condition. However, it is not suit for preparing metal NPs into 3D support. Fortunately, atomic layer deposition (ALD) has been applied to prepare thin film and noble NPs.[28-30] ALD is a thin film deposition technique relied on self-limiting surface reactions, sequential binary reactions between gaseous precursor molecules and a substrate in a layer-by-layer fashion, and it is known for its atomic level thickness control.[28, 31] It has been found that many metals have the tendency to form highly dispersed NPs on oxide or other nonmetal substrates during the initial stage of the ALD process.[32] This is mainly due to the difference in surface energies between the deposited metal and substrate. This so-called Volmer-Weber (islands) growth is therefore a natural and straightforward way to deposit supported metallic NPs.[33] Metal ALD is also a good alternative to wet chemistry techniques because it allows the deposition of the materials to occur on substrates with demanding three-dimensional (3D) surface topologies.[33] In addition, metal ALD have higher utilization of the metal than wet chemistry techniques, because the noble metal could drain in washing process by wet chemistry techniques. More recently, the ALD approach was applied to prepare noble metal NPs catalysts on different support materials such as commercial carbon black powders,[34] carbon nanotubes (CNT) and 3D CNT/graphene hybrid in fuel cell applications.

In this work, three-dimensional graphite-coated nickel foam (GNF) was synthesized by CVD process, and Pd NPs were grown on GNF by Pd ALD technology. The substrate surface morphology was chosen as a crucial factor in nucleate and growing period on metal ALD process.[28] So, the time of CVD process was studied to obtain appropriate substrate for Pd ALD growth. Moreover, the effect of ALD cycles on the Pd loading and its catalytic performance was also investigated. To examine the catalytic performance, the novel ALD-Pd/GNF binder-free electrodes were characterized through the measurement of ethanol electro-oxidation in the alkaline medium.

Experimental section

Preparation of GNF

Similar to that previously reported,[26] GNF was synthesized by CVD using nickel foam as the substrate, methane (CH_4) was used as the carbon source for graphite foam growth under protective atmosphere.[35] In briefly, the Ni foam (NF) was cut into strips of 1.8×10 cm^2 and carefully washed by acetone, ethanol, hydrochloric acid (1 M) and deionized water, then dried in a vacuum. After weighed, the NF was positioned at the center of the quartz tube furnace (KJ Grocp, China). Then filled with argon (Ar) (200 sccm, 99.99%) until the chamber reached atmospheric pressure. The quartz tube furnace was heated to 1000 ℃ at a 10 ℃/min heating rate and maintained for 15 min under atmospheric pressure with a gas flow of H_2/Ar (H_2/Ar = 40 : 200 sccm) to clean the surface of nickel foam. The CH_4 (99.999 %) was introduced 5 min, 10 min and 15 min, respectively. Then the sample is rapidly cooled to the room temperature under Ar flow. Finally, the samples were weighed to ensure content of graphite and denoted as GNF-5, GNF-10, GNF-15, respectively.

ALD of Pd on GNF

Pd NPs were deposited onto GNF support by using metal ALD technology, and this method was performed by following the synthesis method disclosed in Ref.[28] by a little modification. In brief, the Pd NPs were grown on the GNF supports by using Pd(II) hexafluoroacetylacetonate (Pd(hfac)$_2$) and formalin as ALD precursors. The Pd(hfac)$_2$ precursor (Sigma-Aldrich, >97 wt%) contained in a stainless steel bubbler was heated to 50 ℃ to produce a practical vapor pressure. The formalin reducing reagent is a solution of 37 wt% formaldehyde (Changzhen Huabo Instruments Ltd, China) in water with 10-15 wt% methanol as a stabilizer. The regular ALD cycle consisted of a 5 s exposure to $Pd(hfac)_2$, a 5 s N_2 purge, a 10 s exposure to formalin, a 6 s N_2 purge. The Pd NPs were deposited with the support temperature at 200 ℃ at a reactor pressure of 700 mTorr on GNF-5, GNF-10, GNF-15, respectively by 300 ALD cycle. And they were denoted as ALD-Pd/GNF-5, ALD-Pd/GNF-10, ALD-Pd/GNF-15, respectively. Meanwhile, the Pd NPs were deposited on GNF-10 after 150, 300, 450 and 600 ALD cycle, respectively. And they were denoted as 150-ALD-Pd/GNF, 300-ALD-Pd/GNF, 450-ALD-Pd/GNF and 600-ALD-Pd/GNF, respectively. The total synthesis process was illustrated in Fig. 1.

Characterization of GNF and ALD-Pd/GNF catalysts

The chemical composition and morphology of GNF were characterized by X-ray diffraction (XRD, DX-2700, Dandong Ltd, China), field-emission scanning electron microscope (SEM, S-4800) and Raman spectra. The actual Pd contents of ALD-Pd/GNF were determined by Inductively Coupled Plasma-atomic Emission Spectrometry (ICP, IRIS Adv, USA) method. The surface morphology and microstructures of ALD-Pd/GNF were characterized by SEM. Meanwhile, the energy dispersive X-ray spectrometer (EDS, Inca300, Oxford) attached to the SEM was also used to verify the components of ALD-Pd/GNF. X-ray photoelectron spectroscopy (XPS) measurements were performed with monochromatic Al Kα (1486.71 eV) X-ray radiation (15 kV and 10 mA).

The electrochemical measurements of ALD-Pd/GNF were carried out in a conventional three-electrode electrochemical cell on a CHI 760B (Shanghai Chenhua Instruments Ltd, China). The counter and reference electrodes were graphite electrode and Hg/HgO electrode, respectively. The area of ALD-Pd/GNF electrodes was set at 1 cm^2, and it was directly served as working electrode. A commercial Pd/C electrocatalyst (10 wt% Pd loading, Sigma-Aldrich) was used for comparison. The working electrode of commercial Pd/C catalyst was prepared by a conventional method. In brief, the suspension of commercial Pd/C in 1.0 mL deionized water, 1.0 mL isopropanol, and 50 μL of a 5 wt% Nafion solution was mixed by 30 min ultrasonic agitation. 5 μL of commercial Pd/C portion (amount of Pd loading 17.4 $\mu g/cm^2$) suspension was then dropped onto the prepolished glassy carbon electrode (GCE, 0.3 cm in diameter). All potentials reported in this paper were referred to the Hg/HgO. Cyclic voltammetry (CV) measurement was performed under a Ar saturated atmosphere using 1M KOH with or without 1 M ethanol as the electrolyte solution at a scan rate of 50 mV/s. Chronoamperometry (CA) measurement was carried for 1000 s at -0.3 V for the study of relative stability of the electrodes under a Ar saturated atmosphere using 1M KOH with 1M ethanol as the electrolyte solution. Electrochemical impedance spectra (EIS) was also used to analyze ALD-Pd/GNF electrodes under Ar saturated atmosphere using 1M KOH with 1M ethanol as the electrolyte solution. In this paper, the frequency was from 0.1 Hz to 0.1 MHz, and the potential amplitude of AC was the open circuit voltage.

Results and Discussion

To ensure the chemical composition and structure of GNF, XRD was applied. Fig. 2a shows the XRD patterns of under the different CVD time preparation GNF. The three main diffraction peaks at 44.5°, 51.8°and 76.3° in all GNF samples can be ascribed to the diffraction of (111), (200) and (220) planes of Ni, respectively. In addition to diffraction peak of Ni, the diffraction peak located at about 26.4^{o} in all XRD patterns is associated to the (002) of graphite. This indicates that the GNF were synthesized by CVD methods. Fig. 2b shows an SEM image of 3D graphene network coated with Ni. The SEM images (inset of Fig. 2b) show that GNF keep well 3D porous "skeleton/skin" architectures with Ni networks as the skeleton and graphite as the skin. And ripples of graphene were observed on the surface of NF (Fig. 2b). In addition, The GNF was also confirmed by Raman spectrum. Two strong peaks (Fig. 2c) at ~1560 cm^{-1} (G band) and ~2700 cm^{-1} (2D band) are noticed. The intensity ratio of the G/2D band is always used to determine the layer numbers of graphene.[36, 37] Herein, the intensity ratio of G/2D indicates that the GNF only composed of a few layers of graphene. Additionally, it is worth mentioning that the D-band of GNF at ≈ 1350 cm^{-1} is absence, indicating the good quality of GNF.[26]

As well known, metal ALD can grow by islands due to the difference in surface energies between the deposited metal and the substrate.[38, 39] It is useful to prepare nobly metallic NPs for electrocatalysts. Therefore, it is easily deduced that Pd NPs can deposit on GNF to form ALD-Pd/GNF eletrocatalysts by metal ALD technology. Firstly, XRD was applied to detect the chemical composition of as-prepared ALD-Pd/GNF. Suprisingly, the diffraction peaks of Pd have not been discovered, which can be ascribed to the ultralow loading Pd of ALD-Pd/GNF catalysts, corresponding to ICP result (amount of Pd loading is about 23.5 μg/cm^2). Consequently, EDS and XPS were utilized to analyze the chemical composition of

ALD-Pd/GNF. Fig. 3 shows the EDS of the as-prepared ALD-Pd/GNF electrocatalysts. EDS shows the elemental dispersion of C, Ni and Pd in ALD-Pd/GNF. The three elements in the sample were uniformly distributed in the randomly selected area. The white spherical particles (Fig. 3a) can be ascribed to the Pd NPs. Further, XPS was used to determine the surface composition of the ALD-Pd/GNF catalysts. As shown in Fig. 4a, the C 1s (~285 eV) and O 1s (~534 eV) peaks were accompanied by the two Pd 3d peaks. The core level of C1s XPS spectra of ALD Pd/3D-GNF are shown in Fig 4b. The only peak located at 284.8 eV is attributable to graphitic sp^2 (C=C) bonds, which also indicating the GNF was very pure. The core level Pd 3d spectrum of ALD-Pd/GNF displays a doublet signal (Fig. 4c) that are assigned to Pd at 336.1 and 341.3eV for Pd $3d_{5/2}$ and Pd $3d_{3/2}$, respectively. It indicates that Pd is completely in the metallic form (Pd^0). So it is feasible that purely metal NPs can be prepared by metal ALD technology. In addition, the novel catalysis can be some oxidation state by the wet chemistry techniques of preparation, such as PdO in the Pd NPs catalysis.[40, 41] Comparing the wet chemistry techniques, ALD can prepare purely metallic NPs which indicate high the novel metallic utilization. Meanwhile, the Ni diffraction peaks were not discovered by XPS spectrum, and the core level Pd 3d spectrum of ALD-Pd/GNF was not moved, indicating that Pd and Ni can be not formed the PdNi alloy.

Especially, it was found that the morphology and content of graphite of GNF support will greatly affect the growing of Pd NPs. The difference in intensity (inset of Fig. 2a) might be caused by the difference in the CVD time, owning to different content of graphite. Fig. 5 shows the SEM micrograph of the as-prepared catalysts of ALD-Pd/GNF. Three samples maintain better 3D structure from Fig. 5a1, a2 and a3, indicating excellent electrical conductivity of as-prepared catalysts. Interestingly, Fig. 5b1, b2 and b3 indicates that Pd NPs can well distribute in the GNF by Pd ALD progress, and the average particle sizes of Pd NPs are about 20-30 nm. Comparing Fig. 5c1, c2 and c3 (high-magnification SEM images), this is observed that the Pd NPs of ALD-Pd/GNF-10 can be better dispersed than other sample. The results could owe to content of graphite what can disperse Pd NPs in ALD Pd process. Lee et al.[42] discovered that Pd more easily nucleates and disperses on defective sites (dangling bonds) than on the more chemically inert basal planes.[42] The defective number of GNF support can be mainly influenced by content of graphite. The surface of GNF-15 can have less dangling bonds than GNF-10 through increasing the CVD time, indicating inferior dispersity of Pd NPs and larger Pd NPs on the GNF-15 support. Although, there are more defective sites on the GNF-5 because of low content of graphite, Pd NPs appears to segmental agglomeration on the surface of GNF-5 (as shown in Fig. 5c1). The phenomenon can attribute to the weak strength in between Pd NPs and GNF-5. However, it has appropriately dangling bonds on fold belts of the GNF-10 which owe to rough NFs' substrate, Pd NPs can uniformly disperses on the GNF-10. So the better dispersed Pd NPs of ALD-Pd/GNF-10 could owe to the content of graphite. Therefore, it is rationally deduced that content of graphite of GNF-10 take very advantage of Pd homogeneous deposition. Based on above analysis, the as-prepared sample contains pure Pd NPs, and Pd NPs distributed uniformly on GNF support.

Inspired by the attractive structures and composition of the ALD-Pd/GNF, the electrochemical properties of as-prepared catalysts were investigated in the 1M KOH with or without ethanol aqueous solution by CV and CA. Fig. 6a shows the electrochemical property of as-prepared catalysts in 1M KOH solution in the potential range of -0.95 V to +0.15 V at a scan rate of 50 mV/s. An obvious cathodic peak in all CVs at around -0.2 V.vs(Hg/HgO) during the backward sweep was caused by the reduction of the PdO which formed during the forward sweep at positive potential region. It is known that the electrochemical surface area (ECSA) could reveal to what degree of metal (i.e. Pd, Pt) site is utilized, and the higher ECSA can be derived from smaller size of NPs.[43, 44] The ECSA has also been measured by determining the columbic charge for the reduction of palladium oxide. The ECSA was calculated by using the equation follows: ECSA =Q/(SI), Q is the columbic charge, S is a constant (0.405 mC/cm^2), I is the catalyst loading of Pd.[44] The values of the ECSA are summarized in Table S1. High ECSA of ALD-Pd/GNF-10 (63.88 m^2/g_{Pd}) originates from the good dispersion of Pd NPs and probably a good conductivity of the GNF-10. To further confirm the electro-oxidation of ethanol, all electroctalysts are studied in 1M KOH with 1M ethanol in the potential range of -0.95 V to +0.15 V at a scan rate of 50 mV/s. Fig. 6b shows CVs of three as-prepared catalysts for the electro-oxidation of ethanol. It can be observed that all the ALD-Pd/GNF appears to have similar catalytic features that onset and peak potential for the electro-oxidation of ethanol, at around -0.60 V and -0.16 V, respectively. During the forward sweep, two anodic peaks appear for all the catalysts. It is well accepted that the adsorption of OH^- on pure Pd occurs around -0.7 V.vs(Hg/HgO) electrode in alkaline medium.[45] With increasing potential, the current density increases sharply due to striping of adsorbed carbonaceous species by freshly generated Pd-OH. The associated reactions are presented by Eqs. (1-4). At higher potential in-situ generated PdO fully blocks the active sites for the further adsorption of reactive species which lead to the drop of current density.[46-48] Generally speaking, the higher the peak of forward sweep is, the stronger ability to oxidate ethanol has. So comparing current density of three as-prepared catalysts, ALD-Pd/GNF-10 is highest than that of ALD-Pd/GNF-5 (16.9 vs.6.2 mA/cm^2) and ALD-Pd/GNF-15 (16.9 vs.4.2 mA/cm^2). Based on the above analysis, the critical influence should be content of graphite. Different content of graphite might have an effect on Pd deposition and distribution. On backward sweep, the monolayer oxide film is reduced and a hump is obtained in cathodic region followed by an oxidation peak due to oxidation of freshly adsorbed ethanol and previously adsorbed oxidisable intermediates (4).

$$Pd + CH_3CH_2OH \leftrightarrow Pd\text{-}(CH_3CH_2OH)_{ads} \qquad (1)$$

$$Pd\text{-}(CH_3CH_2OH)_{ads} + 3OH^- \rightarrow Pd\text{-}(CH_3CO)_{ads} + 3H_2O + 3e^- \qquad (2)$$

$$Pd\text{-}(CH_3CO)_{ads} + Pd\text{-}OH_{ads} \rightarrow Pd\text{-}CH_3COOH + Pd \qquad (3)$$

$$Pd\text{-}CH_3COOH + OH^- \rightarrow Pd + CH_3COO^- + H_2O \qquad (4)$$

To further confirm the anti-poisoning ability and stability of the catalysts, the CA test at a constant potential of -0.2 V vs. Hg/HgO was conducted in electrolyte 1 M KOH with 1 M ethanol, as shown in Fig. 6c. Both potentiostatic currents show a quick decay within the first few minutes, resulting from the formation of adsorbed intermediates such as Pd-CO_{ads} and Pd-$(CH_3CH_2OH)_{ads}$ in the electro-oxidation of ethanol. The higher initial current that is observed for ALD-Pd/GNF10 is indicative of a larger number of active sites available for the ethanol oxidation.[49] Afterward, nearly constant currents at longer times are viewed. The ALD-Pd/GNF-10 displays higher current plateau, indicating more catalytically active surface area, better CO tolerance and well stability in ethanol oxidation.[34] However, the stability and anti-poisoning ability of as-prepared catalysts are not very good as shown in CA curves (after 4000s), due to the single Pd NPs of as-prepared catalysts. As well know, single noble metal NPs usually present the low stability and anti-poisoning ability of catalysts.

To provide more insight into the ethanol oxidation behavior on the as-prepared electrodes, EIS was applied in this study to investigate the mechanism of ethanol oxidation. The different impedance behaviors in different potential regions reveal that the mechanism and rate-determining-step (r.d.s) in ethanol electro-oxidation. A EIS test at a frequency range from 0.1Hz to 0.1MHz was conducted in electrolyte 1M KOH with 1M ethanol. Fig. 7a represents the EIS plots of as-prepared electrodes. It shows that the ALD-Pd/GNF-10 catalysts have the smallest the diameters of the arcs than that of ALD-Pd/GNF-5 and ALD-Pd/GNF-15, suggesting polarization resistance and fast the rate of the mass transport within the ALD-Pd/GNF-10 electrodes. Inset of Fig. 7a indicates that ALD-Pd/GNF-10 have lower the ohmic resistance than other ALD-Pd/GNF. These results suggest that ALD-Pd/GNF-10 can be more effective to electro-oxidate ethanol than other ALD-Pd/GNF. Based on the impedance results, the equivalent circuit shown in Fig. 7b was used to fit the EIS data. In the equivalent circuit, Constant-phase element (CPE) is the double-layer capacitance, R_s and R_{ct} are the solution resistance and charge-transfer resistance, respectively.[50, 51] The values of R_S, CPE and R_{CT} were calculated from the CNLS fitting of the experimental impedance spectra and their resulting values are listed in Table S2.

Based on the above analysis, Pd NPs can well grow on GNF with metal ALD technology, but metal ALD cycle also plays a key role in the metal NPs nucleation and growth process. To further explore the influence of the Pd ALD cycle, we prepared four samples under different ALD Pd cycle on GNF-10 support. Fig. 8 shows the SEM images of the four as-prepared catalysts. Low-magnification SEM images (Fig. 8a1, a2, a3 and a4) indicate that as-prepared catalysts keep also well 3D structure, ensuring excellent electrical conductivity. Compared to high-magnification SEM images (Fig. 8b1, b2, b3 and b4), Pd NPs are more and more large with increasing Pd ALD cycle. And the average crystallite size of the 150 ALD-Pd/GNF, 300 ALD-Pd/GNF, 450 ALD-Pd/GNF and 600 ALD-Pd/GNF catalysts falls in the range of 10-15 nm, 20-25nm, 30-35nm and 40-50nm, respectively. Fig.8b4 shows that Pd NPs appear uneven with sectional agglomeration, when Pd ALD cycles go over 450 cycles. This indicates that the optimized cycle of Pd ALD for preparing Pd NPs on GNF is 450 cycle.

The actual Pd mass compound of ALD-Pd/GNF was determined by ICP method. Fig. 9 shows the evolution of the Pd mass compound as a function of the number of Pd ALD cycle. Before 150 cycles, Pd NPs are in the stage of nucleation, so Pd mass compound is very low (about 1.41 μg/cm²). This brings into correspondence with Ref.[52] that ALD Pd have a long nucleation periods around 30–120 cycles. After 150 cycles, the average compound of the Pd increases linearly with the number of ALD Pd cycle, implying a constant rate of the Pd growth. And the growth rate of Pd on GNF support was about 0.12±0.01 μg/cm² per cycle (the ICP results are presented in Table 1), due to its self-limiting surface chemistry during alternating precursor and coreactant pulses.[53]

Based on the above results, we tested the as-prepared catalysts in 1M KOH with or without 1M ethanol to study its electrocatalytic ability. Firstly, the as-prepared catalysts were tested in 1M KOH electrolyte solution to study the ECSA. Fig. 10a shows the electrochemical property of as-prepared catalysts and commercial Pd/C in 1M KOH solution in the potential range of -0.95 V to +0.15 V at a scan rate of 50 mV/s. Compared five curves, the 450-ALD-Pd/GNF exhibits large cathodic peaking area at around -0.2 V.vs(Hg/HgO) during the backward sweep, indicating high ECSA. The values of the ECSA are summarized in Table 1. But the 150-ALD-Pd/GNF presented the highest ECSA, which owed to the good dispersion of Pd NPs and small Pd particle size, corresponding with the SEM result. And the ECSA become declining when ALD cycles were increased, indicating more and more low catalytic activity. To further confirm the electro-oxidation of ethanol, all as-prepared catalysts and commercial Pd/C are studied in 1M KOH with 1M ethanol in the potential range of -0.95 V to +0.15 V at a scan rate of 50 mV/s. Fig. 10b shows CVs of four as-prepared catalysts and commercial Pd/C for the electro-oxidation of ethanol. It can be observed that peaking current density rise continually with ALD Pd cycle increasing before 450 cycles. But with the Pd ALD cycle sequential increase, the current density become declining. As explained in SEM, sectional Pd NPs appear agglomeration while Pd ALD cycles are greater than 450 cycles. Therefore, the current density of 600-ALD-Pd/GNF catalysts become declining. All the comparative electrochemical data are presented in Table 2. To further investigate the anti-poisoning ability and short term stability of the four catalysts, CA curves on the four samples and commercial Pd/C toward ethanol oxidation were conducted at -0.2 V for a period of time (4000 s, as shown in Fig. 10c). In the region of activation polarization, the 450-ALD-Pd/GNF exhibits the highest current density. So far, it is demonstrated that 450-ALD-Pd/GNF exhibits best catalytic activity for ethanol oxidation. Comparing to commercial Pd/C catalyst, the peaking current density of 450-ALD-Pd/GNF (about 39.97 mA/cm^2) is about 2.64 times. The high catalytic activity of ALD-Pd/GNF should be attributed to the low diffusion resistance and high conductivity of GNF support and the highly dispersed ALD-Pd NPs. Meanwhile, we also compare the experimental conditions, certain morphologies, catalytic activity, etc. with this work and previous work on Pd, PdNi catalysts reported in recent literatures (as shown in Table S3).

Conclusion

In summary, a novel GNF was synthesized by the CVD method. The GNF can serve as a good support for noble electrocatalysis application, because it contains unique 3D structure and excellent electrical conductivity. Based on these advantages, ultralow loading (below 50 μg/cm^2 $_{Pd}$) Pd NPs were successfully prepared by ALD technology on GNF support for the first time. The as-prepared catalysts of ALD-Pd/GNF exhibited a significantly high catalytic activity for the ethanol oxidation in alkaline media. Especially, it was discovered that content of graphite was very important for the dispersity of Pd NPs under the same Pd ALD condition. When CVD time for preparing GNF was 10 min, the ALD-Pd/GNF-10 catalysts (peaking current density was about 16.9 mA/cm^2) showed higher electro-catalytic performances than other as-prepared catalysts (6.2 mA/cm^2 and 4.2 mA/cm^2 of ALD-Pd/GNF-5, ALD-Pd/GNF15, respectively) for the electro-oxidation of ethanol. In addition, cycle of Pd ALD was researched, because it regulated the Pd NPs nucleation and growth. The as-prepared catalysts exhibited an excellent catalytic activity for the ethanol oxidation when cycle of ALD Pd was 450 cycle. The peaking current density of 450 ALD-Pd/GNF was about 2.64 times (about 39.97 mA/cm^2) as high as that of commercial Pd/C (about 15.17 mA/cm^2). The Pd ALD technology is a promising method to effectively deposit nanometer catalysts with ultralow loading onto 3D porous support which can be directly employed as the electrode of fuel cells.

Acknowledgments

This work is supported by the National Natural Science Foundation of China (NSFC, 21306119), the Provincial Natural Science Foundation of Sichuan (2013FZ0034, 2013JY0150), the Outstanding Young Scientist Foundation of Sichuan University (2013SCU04A23).

References

1. F.-M. Li, X.-Q. Gao, S.-N. Li, Y. Chen and J.-M. Lee, *NPG Asia Materials*, 2015, **7**, e219.
2. P. Wu, Y. Huang, L. Kang, M. Wu and Y. Wang, *Sci Rep*, 2015, **5**, 14173.
3. F. Miao, B. Tao and P. K. Chu, *Dalton Trans*, 2012, **41**, 5055-5059.
4. X. Yang, Q. Yang, J. Xu and C.-S. Lee, *Journal of Materials Chemistry*, 2012, **22**, 8057.
5. E. Antolini, *Journal of Power Sources*, 2007, **170**, 1-12.
6. K. Zhang, D. Bin, B. Yang, C. Wang, F. Ren and Y. Du, *Nanoscale*, 2015, **7**, 12445-12451.
7. Z.-Y. Zhou, Q. Wang, J.-L. Lin, N. Tian and S.-G. Sun, *Electrochimica Acta*, 2010, **55**, 7995-7999.
8. K. Wu, X. Mao, Y. Liang, Y. Chen, Y. Tang, Y. Zhou, J. Lin, C. Ma and T. Lu, *Journal of Power Sources*, 2012, **219**, 258-262.
9. E. Antolini, *Energy & Environmental Science*, 2009, **2**, 915.
10. S. J. Ye, D. Y. Kim, S. W. Kang, K. W. Choi, S. W. Han and O. O. Park, *Nanoscale*, 2014, **6**, 4182.
11. H. Liu, W. Li and A. Manthiram, *Applied Catalysis B: Environmental*, 2009, **90**, 184-194.
12. J. Chen, Y. Li, S. Liu, G. Wang, J. Tian, C. Jiang, S. Zhu and R. Wang, *Applied Surface Science*, 2013, **287**, 457-460.
13. E. J. Lim, Y. Kim, S. M. Choi, S. Lee, Y. Noh and W. B. Kim, *J. Mater. Chem. A*, 2015, **3**, 5491-5500.
14. X. Yang, M. Zhen, G. Li, X. Liu, X. Wang, C. Shu, L. Jiang and C. Wang, *Journal of Materials Chemistry A*, 2013, **1**, 8105.
15. V. M. Shinde, E. Skupien and M. Makkee, *Catal. Sci. Technol.*, 2015, **5**, 4144-4153.
16. J. Zhang, Y. Cheng, S. Lu, L. Jia, P. K. Shen and S. P. Jiang, *Chemical communications*, 2014, **50**, 13732-13734.
17. Q. W. Baocang Liu, Shengli Yu, Peng Jing, Lixia Liu, Guangran Xua and Jun Zhang, *Nanoscale*, 2014, **6**, 11887–11897.
18. Z. Zhang, Y. Dong, L. Wang and S. Wang, *Chemical communications*, 2015, **51**, 8357-8360.
19. C.-H. A. Tsang, K. N. Hui, K. S. Hui and L. Ren, *J. Mater. Chem. A*, 2014, **2**, 17986-17993.
20. C. Hu, X. Zhai, Y. Zhao, K. Bian, J. Zhang, L. Qu, H. Zhang and H. Luo, *Nanoscale*, 2014, **6**, 2768.
21. R. Yue, H. Wang, D. Bin, J. Xu, Y. Du, W. Lu and J. Guo, *J. Mater.*

Chem. A, 2015, **3**, 1077-1088.

22. P. S. Roy, J. Bagchi and S. K. Bhattacharya, *Catalysis Science & Technology*, 2012, **2**, 2302.
23. Q. Tan, C. Du, Y. Sun, L. Du, G. Yin and Y. Gao, *Nanoscale*, 2015, **7**, 13656-13662.
24. Y. Z. Xianjun Zhu, Shanthi Murali, Meryl D. Stoller Rodney S. Ruoff, *ACS nano*, 2011, **5**, 3333-3338.
25. N. Li, Z. Chen, W. Ren, F. Li and H. M. Cheng, *Proceedings of the National Academy of Sciences*, 2012, **109**, 17360-17365.
26. X. Cao, Y. Shi, W. Shi, G. Lu, X. Huang, Q. Yan, Q. Zhang and H. Zhang, *Small*, 2011, **7**, 3163-3168.
27. X. Liang, L. B. Lyon, Y.-B. Jiang and A. W. Weimer, *Journal of Nanoparticle Research*, 2012, **14**.
28. J. Lu and P. C. Stair, *Langmuir*, 2010, **26**, 16486-16495.
29. D. N. Goldstein and S. M. George, *Thin Solid Films*, 2011, **519**, 5339-5347.
30. J. Lu, B. Fu, M. C. Kung, G. Xiao, J. W. Elam, H. H. Kung and P. C. Stair, *Science*, 2012, **335**, 1205-1208.
31. C.-T. Hsieh, Y.-Y. Liu, D.-Y. Tzou and W.-Y. Chen, *The Journal of Physical Chemistry C*, 2012, **116**, 26735-26743.
32. P. C. Stair, *The Journal of chemical physics*, 2008, **128**, 182507.
33. M. J. Weber, A. J. M. Mackus, M. A. Verheijen, C. van der Marel and W. M. M. Kessels, *Chemistry of Materials*, 2012, **24**, 2973-2977.
34. R.-S. Juang, C.-T. Hsieh, J.-Q. Hsiao, H.-T. Hsiao, D.-Y. Tzou and M. M. Huq, *Journal of Power Sources*, 2015, **275**, 845-851.
35. H. Ji, L. Zhang, M. T. Pettes, H. Li, S. Chen, L. Shi, R. Piner and R. S. Ruoff, *Nano Lett*, 2012, **12**, 2446-2451.
36. X. Xia, D. Chao, Z. Fan, C. Guan, X. Cao, H. Zhang and H. J. Fan, *Nano letters*, 2014, **14**, 1651-1658.
37. B.-M. Goh, Y. Wang, M. V. Reddy, Y. L. Ding, L. Lu, C. Bunker and K. P. Loh, *ACS Applied Materials & Interfaces*, 2014, **6**, 9835-9841.
38. A. W. Jeffrey S. King, Juergen Biener, Sergei O. Kucheyev, Yinmin M. Wang, Theodore F. Baumann‡ Sandeep K. Giri, Alex V. Hamza, Marcus Baeumer, Stacey F. Bent, *Nano letters*, 2008, **8**, 2405-2408.
39. J. Li, X. Liang, D. M. King, Y.-B. Jiang and A. W. Weimer, *Applied Catalysis B: Environmental*, 2010, **97**, 220-226.
40. M. S. Ahmed and S. Jeon, *Journal of Power Sources*, 2015, **282**, 479-488.
41. J. E. Choe, M. S. Ahmed and S. Jeon, *Journal of Power Sources*, 2015, **281**, 211-218.
42. H.-B.-R. Lee, S. H. Baeck, T. F. Jaramillo and S. F. Bent, *Nano letters*, 2013, **13**, 457-463.
43. W. Wang, Y. Yang, Y. Liu, Z. Zhang, W. Dong and Z. Lei, *Journal of Power Sources*, 2015, **273**, 631-637.

44. Y. Liu, W. Wang, Y. Yang, F. Wang, X. Zhao and Z. Lei, *Applied Catalysis A: General*, 2015, **505**, 410-415.

45. J. Bagchi and S. K. Bhattacharya, *Transition Metal Chemistry*, 2007, **33**, 113-120.

46. F. Gobal and R. Arab, *Journal of Electroanalytical Chemistry*, 2010, **647**, 66-73.

47. Z. X. Liang, T. S. Zhao, J. B. Xu and L. D. Zhu, *Electrochimica Acta*, 2009, **54**, 2203-2208.

48. P. Mukherjee, P. S. Roy, K. Mandal, D. Bhattacharjee, S. Dasgupta and S. K. Bhattacharya, *Electrochimica Acta*, 2015, **154**, 447-455.

49. Q. M. Qingming Shen, Jianjun Shi, Liping Jiang, Jian-Rong Zhang, Wenhua Hou, Jun-Jie Zhu, *J. Phys. Chem. C*, 2009, **113**, 1267–1273.

50. D. Z. Fangfang Zhang, Zejie Zhang, Mingda Zhou Qian Wang, *RSC Advances*, 2015, **5**, 91829–91835.

51. Y. W. T. Q. Zhijun Jia, *RSC Advances*, 2015, **5**, 83314–83319.

52. J. W. Elam, A. Zinovev, C. Y. Han, H. H. Wang, U. Welp, J. N. Hryn and M. J. Pellin, *Thin Solid Films*, 2006, **515**, 1664-1673.

53. M. J. Weber, A. J. M. Mackus, M. A. Verheijen, V. Longo, A. A. Bol and W. M. M. Kessels, *The Journal of Physical Chemistry C*, 2014, **118**, 8702-8711.

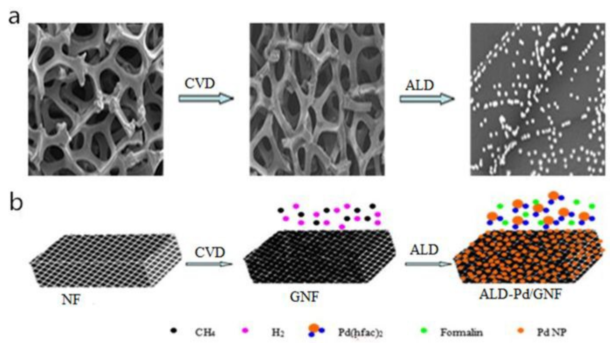

Fig.1 An illustration of the formation of ALD-Pd/GNF (a) actually prepared results and (b) schematic illustration of the prepared process of ALD-Pd/GNF.

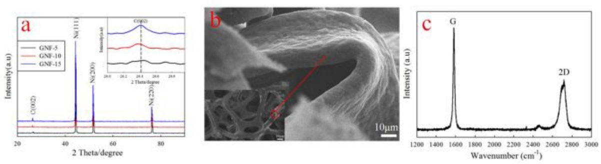

Fig. 2 (a) XRD patterns of the GNF. (b) high-magnification SEM image of GNF. Inset: low-magnification SEM image of GNF. (c) Raman spectra of GNF.

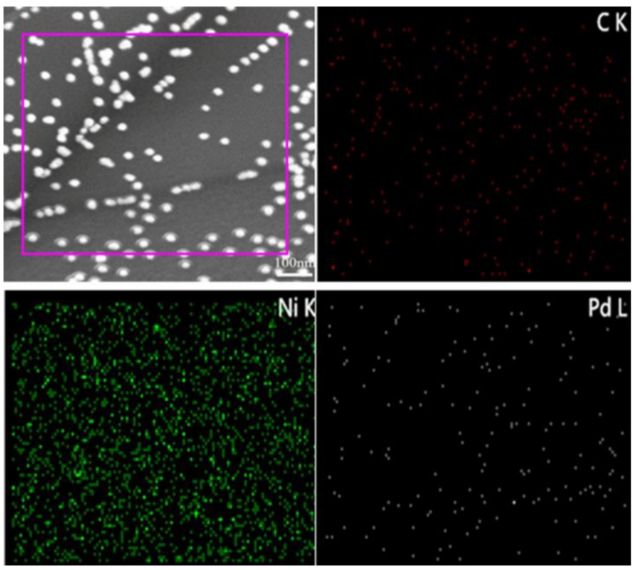

Fig.3 The elemental mapping of ALD-Pd/GNF.

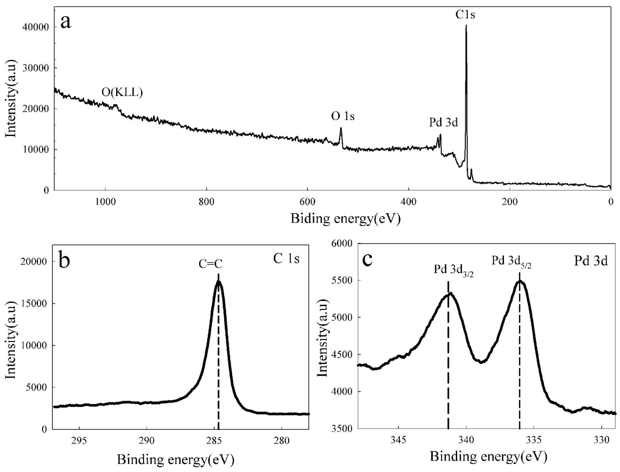

Fig.4 The XPS spectra (a) core level of C1s (b) and Pd3d (c) spectra of the ALD-Pd/GNF.

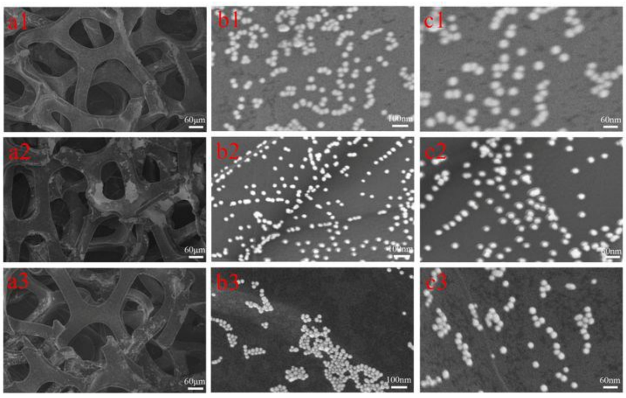

Fig. 5 Low- and high-magnification SEM images of (a1-c1) ALD-Pd/GNF-5, (a2-c2) ALD-Pd/GNF-10 and (a3-c3) ALD-Pd/GNF-15.

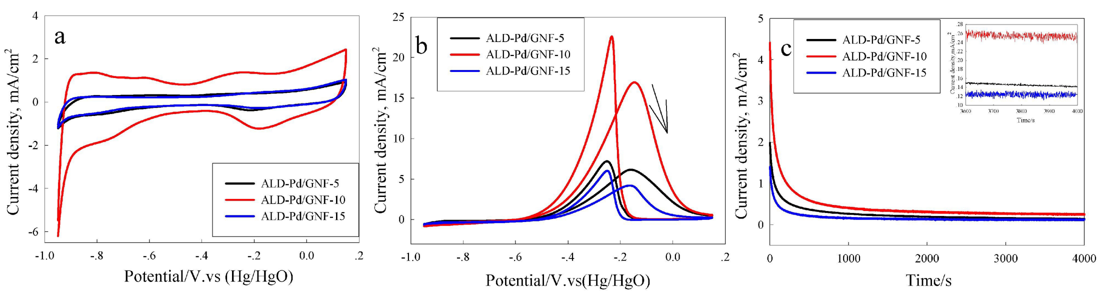

Fig.6 CV curves of the ALD-Pd/GNF-5, ALD-Pd/GNF-10 and ALD-Pd/GNF-15 in 1 M KOH solution (a) and in 1 M KOH with 1 M ethanol solution (b) saturated

with Ar at a scan rate of 50 mV/s. Chronoamperometric response of the ALD-Pd/GNF-5, ALD-Pd/GNF-10 and ALD-Pd/GNF-15 catalysts (c) and the current density after 4000 s inset of (c) fixed potential: −0.2 V.vs(Hg/HgO).

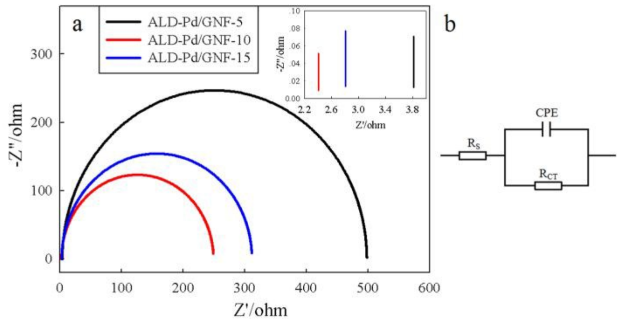

Fig7. (a)EIS curves of the ALD-Pd/GNF-5, ALD-Pd/GNF-10 and ALD-Pd/GNF-15 catalysts measured in 1 M KOH with 1 M ethanol in a frequency range from 0.1Hz to 0.1MHz. (b) the equivalent electrical circuit.

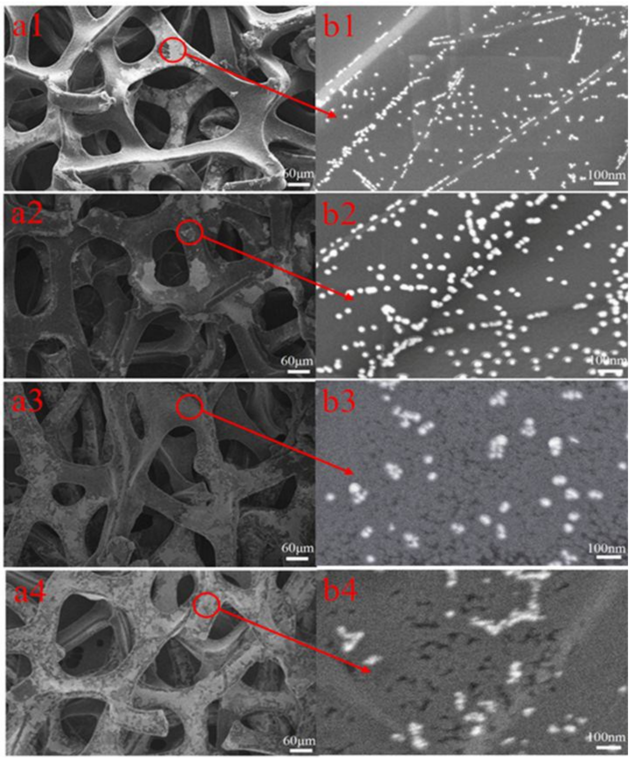

Fig. 8 Low- and high-magnification SEM images of (a1–b1) 150 ALD-Pd/GNF,

(a2-b2) 300 ALD-Pd/GNF, (a3-b3) 450 ALD-Pd/GNF and (a4-b4) 600 ALD-Pd/GNF.

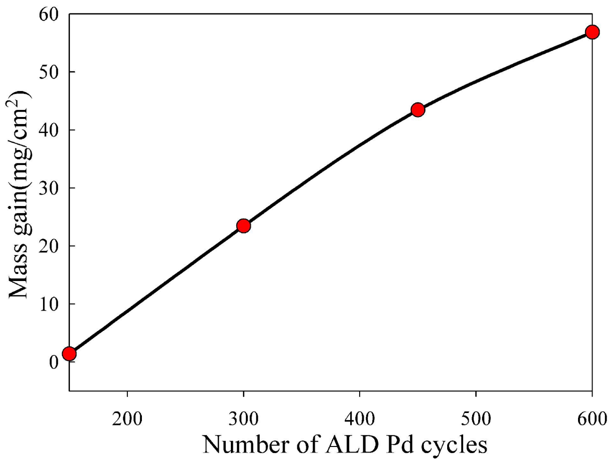

Fig. 9 Average gain of the Pd mass compound determined of four as-prepared sample from the ICP results.

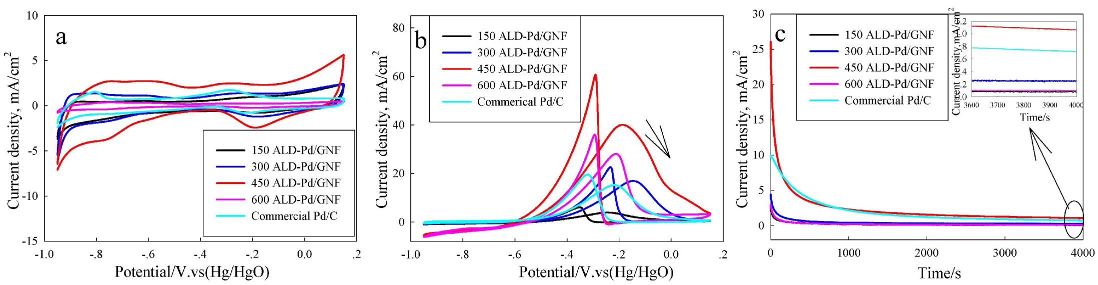

Fig.10 CV curves of the 150 ALD-Pd/GNF, 300 ALD-Pd/GNF, 450 ALD-Pd/GNF, 600 ALD-Pd/GNF and Commercial Pd/C in 1 M KOH solution (a) and in 1 M KOH with 1 M ethanol solution (b) saturated with Ar at a scan rate of 50 mV/s. Chronoamperometric response of the 150 ALD-Pd/GNF, 300 ALD-Pd/GNF, 450 ALD-Pd/GNF, 600 ALD-Pd/GNF and Commercial Pd/C (c) and the current density after 4000 s inset of (c) fixed potential: −0.2 V.vs(Hg/HgO).

Table 1 Comparing to the Pd mass compound and catalytic activity of the as-prepared catalysts and commercial Pd/C.

catalysts	Pd mass compound (μg/cm^2)	ECSA (m^2/g)	Onset potential (mV)	Peaking potential (mV)	Peaking current density (mA/cm^2)
150 ALD-Pd/GNF	1.41	194.49	-601	-245	3.86
300 ALD-Pd/GNF	23.46	63.88	-598	-149	16.93
450 ALD-Pd/GNF	43.44	58.84	-601	-193	39.97
600 ALD-Pd/GNF	56.83	18.96	-600	-212	28.08
Commercial Pd/C	17.4	47.50	-601	-216	15.17

Graphical abstracts

Ultralow loading palladium nanoparticles was facilely synthesized on three-dimensional graphite-coated nickel foam support by metal atomic layer deposition technology and used as a promising catalyst for ethanol electro-oxidation reaction.

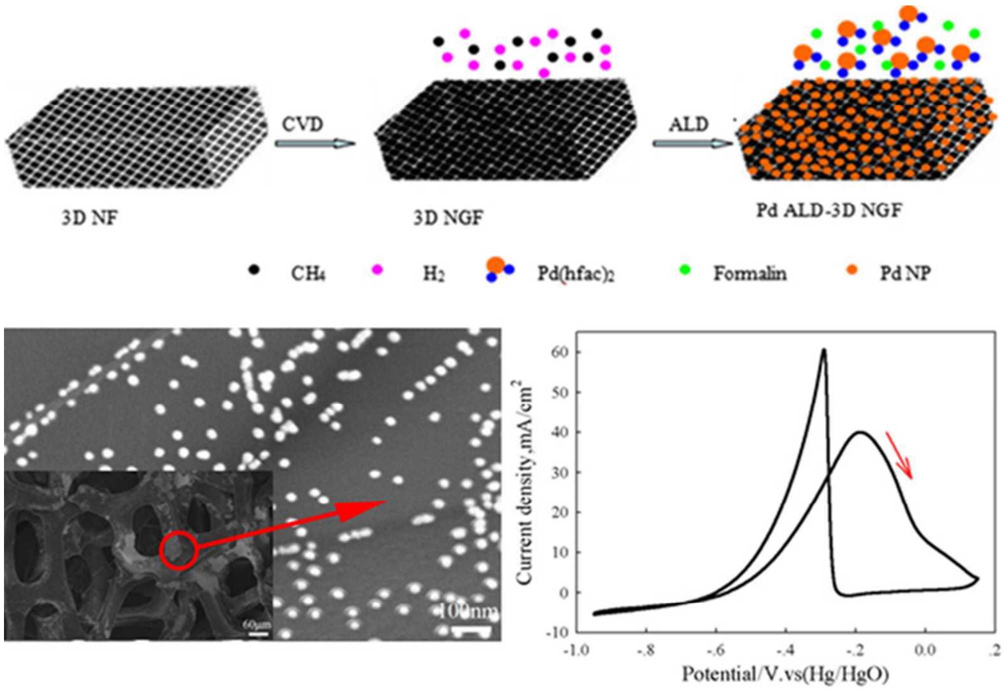

57x40mm (300 x 300 DPI)